Title: Alpha-synuclein overexpression reduces neural activity within a basal ganglia vocal nucleus in a zebra finch model

Running title: Alpha-synuclein overexpression reduces neural activity in a finch song nucleus

Brian R. Dominguez[1], Gabriel Holguin[2], Madeleine S. Daly[1], Reed T. Bjork[1], Stephen L. Cowen[2,3], and Julie E. Miller*[1,4]

[1]Department of Neuroscience, University of Arizona, Tucson, Arizona, United States of America.
[2]Department of Psychology, University of Arizona, Tucson, Arizona, United States of America.
[3]Evelyn F. McKnight Brain Institute, University of Arizona, Tucson, Arizona, United States of America
[4]Departments of Speech, Language and Hearing Sciences, Neurology, and the BIO5 Institute, Tucson, Arizona, United States of America.

***Corresponding Author:**

Julie E. Miller, Ph.D.; E-mail: juliemiller@arizona.edu

Declaration of Competing Interest: J.E. Miller is a 2025 member of the "T2 Targets to Therapies" advisory working group for the Michael J. Fox Foundation for Parkinson's Research.

Other author emails:
Dominguezbrian2@gmail.com
gholguin@scripps.edu
madeleinedaly@arizona.edu
bjork2@arizona.edu
scowen@arizona.edu

Abstract

Vocal motor impairments, including changes in pitch, loudness, and timing are prevalent in Parkinson's Disease (PD) and a target for early intervention and treatment, yet the neural mechanisms underlying these impairments are not understood, motivating work in animal models. The adult male zebra finch songbird is uniquely poised for these studies given vocally-dedicated brain nuclei and a quantifiable output (birdsong). Our prior publication revealed that injection of an adeno-associated virus (AAV5) expressing the human (h) alpha-synuclein (h*SNCA*, a-syn) gene into basal ganglia vocal nucleus Area X results in higher levels of insoluble a-syn protein and changes reminiscent of human PD including softer, shorter, and reduced number of vocalizations compared to AAV5 controls. Here, we test the hypothesis that AAV-h*SNCA* overexpression reduces the firing rate of specific neuronal sub-types in Area X using *in vivo* recordings in anesthetized finches. Five classes of neurons were differentiated in AAV-treated finches based on waveform width (narrow vs. wide) and firing rates (low vs. fast). Wide-waveform/low-rate activity is a consistent feature of striatal medium spiny neurons (MSNs), a dominant cell type in Area X and in mammalian basal ganglia. Reduced firing rates and enhanced post-peak rebound were detected in the AAV-h*SNCA* group for putative MSN neurons compared to AAV controls. No differences in firing rate nor waveform shape were detected for the narrow waveform neurons. Our findings provide the first characterization of early a-syn-driven neural activity changes in vocal control neurocircuitry.

Key words: Parkinson's, alpha-synuclein, zebra finch, songbird, vocal, basal ganglia

34 # Introduction:

35 Pathological accumulation of alpha-synuclein (a-syn) is believed to contribute to
36 multiple neurodegenerative diseases, including Parkinson's disease (PD). Accumulation
37 of toxic a-syn species culminates in the development of Lewy Bodies and Lewy Neurites
38 that are detected in inherited and sporadic cases of PD, dementia with Lewy Body
39 disease, and Multiple Systems Atrophy (1-5). How abnormal increases in a-syn protein
40 expression and its aggregation disrupts ongoing neuronal activity in the basal ganglia
41 (BG) is not understood, yet this information is critical to developing cell-specific
42 therapeutic targets (6-8). One strategy is to examine how elevated a-syn protein interferes
43 with the ongoing firing activity of striatal neurons.

44 Elevated levels of a-syn protein at cortico-striatal synapses can result in synaptic
45 failure and loss of cortico-striatal plasticity based on electrophysiological recordings from
46 rodent brain slices (6-11). Striatal Medium Spiny Neurons (MSNs) show alterations in
47 dendritic spine density, interactions between a-syn aggregates and their NMDA
48 receptors, and reduced efficacy of cortical pre-synaptic glutamatergic input that affects
49 their firing rate (12-15). Furthermore, burst firing is a characteristic feature of MSNs (16),
50 and dysregulated MSN burst firing may contribute to PD as shown in 6-hydroxydopamine
51 (6-OHDA) models (17). A recent study used induced human pluripotent stem cells from
52 patients with Multiple System Atrophy of the Parkinsonian type that were differentiated
53 into MSNs. These MSNs showed hypoexcitability in the form of reduced spontaneous
54 firing rates and reduced frequency and amplitude of miniature post-synaptic currents.
55 These changes were also associated with elevated a-syn release (18). How *in vivo* cell-
56 specific neuronal firing patterns in the basal ganglia relates to the behavioral output is

57 unclear and a critical gap. The scant literature on *in vivo* recordings in rodent h*SNCA*
58 overexpression models comes from nigral, thalamic, and hippocampal neurons
59 evaluating movement and cognition (19-21). Pairing electrophysiological changes in
60 basal ganglia circuitry with vocal behavior offers an early and critical entry-point into
61 furthering our understanding of the effects of alpha-synucleinopathies on neural circuits.

62 Voice and speech deficits are prevalent in PD, impacting communication and
63 quality of life for at least 90% of individuals (22, 23). Early stage vocal deficits (a soft,
64 monotonous voice, altered speaking rate) often arise years before the limb motor
65 symptoms, offering strong potential as an early diagnostic tool, strengthened by insights
66 using machine learning algorithms and smartphone applications (24-37). Our group and
67 others have modeled PD-related vocal deficits using pharmacological and genetic
68 approaches in rodents and songbirds with data from these experiments implicating the
69 h*SNCA* gene in driving early vocal dysfunction (38-46).

70 Songbird models offer distinct advantages over rodents in exploring how the brain
71 encodes sensory and motor information, shaping vocal learning and production in
72 response to feedback (47). In the zebra finch species, the males sing and the females do
73 not. The male song control system in the brain **(Fig 1A**) has strikingly similar neural
74 organization and physiology of the basal ganglia to mammalian species (48-50). Several
75 reviews detail the anatomical, developmental, genetic, functional, and
76 electrophysiological features of this system and their close similarity to human speech
77 and auditory centers in the human brain (51-57). Vocal learning and on-going song
78 modification in the zebra finch model can be investigated through the anterior forebrain
79 pathway (AFP), a structure homologous to the cortico-basal ganglia-thalamo-cortical loop

in humans and other mammals (50). Song-dedicated brain region Area X in the basal ganglia shows high genetic similarity to the striatum, a major human speech control area, and to mammalian neuronal populations (48, 54, 58, 59).

Fig 1A. Finch song control circuitry. Song-dedicated brain nuclei in male finch are shown (HVC and Area X: proper names; RA: robust nucleus of the Arcopallium, lMAN: lateral magnocellular nucleus of the anterior nidopallium). Solid lines: cortico-brainstem circuits for vocal production (finch: HVC to RA to brainstem); dashed lines: cortico-basal ganglia-thalamo-cortico circuits for on-going vocal learning and refinement (lMAN-Area X-DLM-lMAN). Cx – cortex. BG – basal ganglia. DLM – dorsal medial nucleus of the thalamus. Th – thalamus. MB – midbrain. HB – hindbrain. Cb – cerebellum. OB – olfactory bulb. Area X (violet) contains striatal, globus pallidus, and interneurons whereas human BG has separate striatal and pallidal areas. Auditory input (not shown) to finch vocal nuclei is also well-studied (60, 61). Figure modified from Medina et al. (2022).

Electrophysiological recordings in singing finches and anatomical tracings show that MSNs are the *dominant cell type* in Area X and drive the responses of globus pallidus-like (PAL) projection neurons (50, 58, 62). As in mammals, MSNs receive glutamatergic (Glu) inputs from cortex, and globus-pallidus (GP, PAL) type neurons project to the thalamus which then relays input back to the cortex. In the song control system (**Fig 1A**), cortical song nuclei HVC and lMAN provide Glu input to GABAergic MSNs and PAL neurons within Area X (63). While studies of MSN activity in animal models and humans

103 are difficult due to low spontaneous activity (14, 64), finch MSNs are dynamically active
104 during singing and show temporally precise relationships to song structure (62, 65).
105 The PAL nerve terminals end in the dorsal medial thalamic nucleus (DLM) (63).
106 DLM projections to a neuronal sub-population within the premotor nucleus, HVC, can also
107 modulate syllable transitions (66). High tonic firing in these PAL neurons inhibits DLM,
108 reducing excitation onto lMAN and then song nucleus RA, leading to altered song output
109 including variations in pitch (55, 62). Area X and lMAN neurons exhibit firing variability
110 that is related to birdsong features (55, 62). The well-characterized neuronal populations
111 in these brain nuclei and circuitry connections make this a powerful model to study the
112 impact of alpha-synucleinopathies on vocalizations.
113 In our prior work, we showed that targeting Area X with an adeno-associated virus
114 (AAV) drives increased expression of the human (h) wild-type *SNCA* gene leading to PD-
115 like changes in the song – including decreased vocalizations (singing), duration, and a
116 softer, more monotonous vocal output (45). We also showed that a-syn overexpression
117 results in protein aggregates in Area X cell bodies (46). Here, as a critical first step, we
118 categorize cell-specific firing patterns and waveforms in Area X that are affected by a-syn
119 overexpression compared to controls using tetrode recordings in anesthetized finches
120 immediately following singing behavior. Our working hypothesis (**Fig. 1B**) is that h*SNCA*
121 overexpression in Area X will decrease firing rates and alter burst-firing in putative Area
122 X MSNs. We tested this hypothesis by recording from Area X neurons in anesthetized
123 zebra finches.
124
125

126 **Fig 1B**. **Hypothetical model for a-syn driven changes in neural activity in Area X**
127 **and consequences on song control circuitry.** Cortical vocal nuclei (lMAN, HVC)
128 provide glutamatergic (Glu) input to Area X neurons. Striatal Area X MSNs provide
129 GABAergic input to globus-pallidus like (GP, PAL) neurons including those that inhibit
130 thalamic nucleus DLM. Here, we *predict* that abnormally elevated levels of AAV-driven a-
131 syn protein in Area X could alter intrinsic membrane properties of MSNs and/or reduce
132 Glu input to MSNs. Consequently, MSNs would reduce their firing rate (red arrow),
133 leading to increased PAL projection neuron firing and increased inhibition of DLM.
134 Increased DLM inhibition could be responsible for reduced singing and changes in
135 amplitude (loudness) and duration of the song syllables in finches with the AAV-h*SNCA*
136 phenotype (45).

137

138 # Materials and Methods:

139 **2.1. Finch subjects, song recording and analyses.** All animal use was
140 approved by the Institutional Care and Use Committee at the University of Arizona. **Fig**
141 **1C** shows our experimental workflow and tetrode array.

142

143

144 **Fig 1C. Tetrode array and experimental timeline.** Schematic of AAV constructs and
145 coronal section showing bilateral song nucleus Area X (purple) from Medina et al. (2022).
146 Song was collected within three days of the bilateral injection into Area X and then again
147 at two months post-virus injection followed by tetrode recordings in anesthetized finches
148 within five days. At the end of the recording morning, the finch was humanely euthanized,

149 and the brain removed post-mortem for cryosectioning followed by immunohistochemistry
150 to confirm AAV and a-syn protein expression along with tetrode placement.
151
152 Animal procedures followed Medina et al. (2022). Adult non-breeding male zebra finches
153 (approx. 197-365 days post-hatch at time of euthanasia) were moved into individual
154 sound attenuation chambers (Eckel Noise Control Technologies) and acclimated under a
155 14:10 h light-dark cycle for at least two days prior to song recordings and neurosurgery.
156 Behavioral experiments were conducted in the morning from lights-on for two hours to
157 minimize effects of circadian rhythms on gene expression within Area X and to match our
158 prior study (45) along with ensuring singing-driven neuronal activity just prior to
159 conducting the tetrode recordings in anesthetized finches. Songs were acquired from
160 individual males singing alone (known as undirected song) using free-field omnidirectional
161 microphones (Shure 93) suspended at set points over the center of the cage, connected
162 to an audiobox (Audiobox: 44.1 kHz sampling rate per 24-bit depth; Niles, IL) and
163 recorded with Sound Analysis Pro 2011 (SAP 2011, (67) http://soundanalysispro.com/).
164 Song data collected and used for this study can be found at the University of Arizona
165 ReData repository upon publication (10.25422/azu.data.27868266). A basic unit of
166 birdsong is defined as a motif; a motif is comprised of a sequence of repeated syllables
167 (**S1 Fig A**). Wav files from the two-hour recording period were joined (Shuang's audio
168 joiner) and then the entire file was viewed in Audacity (https://www.audacityteam.org/).
169 The most frequently occurring motif was then identified in the joined wav file for two pre-
170 surgical mornings (time point 0) and then two post-surgical mornings (time point, 2
171 months, **Fig 1C**) by an investigator blind to the AAV condition. The two-month timepoint
172 was selected as the endpoint for tetrode recordings because of our prior publication

173 showing the most prominent song and protein changes occurred at this time point in the
174 AAV-h*SNCA* finches (45, 46). Following morning lights-on, the first motif was identified in
175 the wav file and then 25 consecutive renditions of the individual syllable wav files were
176 exported from Audacity from the four mornings. Up to five unique syllables within a motif
177 for each bird were included in the analyses.
178
179 Syllable wav files were processed in Matlab R2014 using the SAP SAT Tools box
180 with code provided by Dr. Nancy Day (Whitman College) to extract individual acoustic
181 features as a feature batch function. Raw amplitude (intensity) measurements were
182 calibrated based on sound chamber location as in our prior study (68). Mean, standard
183 deviation, and coefficient of variation (CV, standard deviation/mean) were then calculated
184 by averaging 50 scores (25 syllable copies x 2 recording sessions) across time points 0
185 (pre-AAV injection) and 2 months post-AAV injection for each syllable within the bird's
186 motifs to account for natural day to day fluctuations in song. For group level comparisons,
187 a normalization score was obtained per bird by dividing timepoint two months (2) post-
188 injection by pre-injection (0). After verifying that scores were not normally distributed,
189 scores were then compared using the Mann Whitney U test in GraphPad Prism (version
190 10) between AAV-h*SNCA* and AAV-GFP groups for all syllable types combined and then
191 sorted by syllable type (**S1 Table**) given prior findings on a-syn differential effects (45).
192 Syllables were sorted into noisy, mixed, or harmonic categories based on visual
193 inspection and Wiener Entropy (WE) scores following our prior publications (**S1 Fig**) (45,
194 69). We focused our analyses on comparing duration, amplitude, and WE scores between
195 the two AAV groups, and their correlations with the electrophysiological analyses for an

196 individual bird (see section on **Statistics** and **S1-2 Figs**). A subset of these birds was
197 used in our separate publication evaluating regional distribution of a-syn protein in finch
198 song nuclei and linear correlations to syllable features in Area X and lMAN (46).
199 As described in Medina et al. (2022), duration is the length of each syllable (in seconds),
200 and amplitude is the intensity or loudness of the syllable (in decibels-dB). WE is a
201 measure of uniformity in the power spectra (i.e., structure of the syllable), where scores
202 are calculated on a logarithmic scale; noisy syllables have values approaching zero while
203 harmonic syllables have more negative scores (approaching infinity). The coefficient of
204 variation (CV) is calculated by dividing the standard deviation of 50 syllable renditions by
205 the mean score and represents variability across motifs for an acoustic feature,
206 modulated by the lMAN-Area X-DLM-lMAN loop (70).
207
208 **2.2 Viral injections:** An adeno-associated virus (AAV) encoding the h*SNCA* gene
209 (AAV5-CBA-*SNCA*, N = 6) was bilaterally injected into Area X while finches were under
210 isoflurane anesthesia with oxygenation (2-3%, 0.5 liters/min oxygen). A control AAV
211 encoding for green fluorescent protein (AAV5-CBA-eGFP, N = 6) was also bilaterally
212 injected into Area X of a separate control group. Both viruses were under the control of
213 the broad promoter, chicken beta-actin (CBA). For the injections, stereotaxic coordinates
214 were used from the bifurcation of the mid-sagittal sinus: 3.1 mm rostral-caudal, 1.62 mm
215 medio-lateral, a depth of 3.1 mm, and head angle of 40 degrees. These coordinates avoid
216 indirect targeting of song nucleus lMAN with virus as previously described (45). Viruses
217 (AAV5) were made and obtained from the University of North Carolina Viral Vector Core

218 through the support of the Michael J. Fox Foundation for Parkinson's Research
219 (https://www.michaeljfox.org/research-tools).
220 A glass pipette was fitted into a Nanoject II pressure-injector and back-filled with mineral
221 oil, then loaded with either the control or the a-syn virus. Approximately 500 nL of virus
222 was injected at a rate of 27.6 nL/injection every 15 seconds for a total of 18 injections.
223 After five minutes, the pipette was slowly retracted and the tip was visually inspected for
224 clogging. Birds were then returned to their sound chambers following post-operative
225 monitoring and resumed singing within a few hours after surgery.
226

227 ## 2.3 Tetrode Implantation and Electrophysiology

228 **Surgical procedure and implantation:** Approximately two months post-virus
229 injection, finches were anesthetized with isoflurane (2-3%, constant flow rate of 0.5-0.8 L
230 of oxygen/min) and underwent acute electrophysiological recordings of right hemisphere
231 Area X. Breathing rate was monitored throughout the experiment, and an infrared heating
232 pad (Kent Scientific) maintained body temperature at 37ºC. The same stereotaxic
233 coordinates were used for the AAV injections targeting Area X. **Ground wire insertion:**
234 A ground/reference wire was inserted into the left hemisphere, contralateral to the virus
235 injection site (mid-sagittal sinus: 3.1 mm rostral-caudal, 1.62 mm medio-lateral). After
236 performing the craniotomy, the dura was pierced with a 30G needle, and the end of the
237 ground wire was lowered to a depth of 2-3 mm. Gel superglue was used to secure the
238 wire to the acid-etched skull (acid from the Metabond kit). Zip Kicker (Pacer Technology)
239 was used to rapidly cure the superglue. **Electrode array insertion:** The existing
240 craniotomy on the right hemisphere (used for virus injection) was expanded to a diameter

241 of ~1.5 mm to better accommodate the electrode array and to have access to dura that
242 was undamaged during virus injection. Tetrode position was confirmed in Area X post-
243 mortem following electrophysiological recordings (**Fig 2**).
244
245 **Electrophysiological recordings:** Neurons from Area X were recorded using a
246 custom-made 800 μm diameter tetrode array composed of 8 twisted-wire tetrodes.
247 Tetrodes were constructed from polyamide-insulated nickel chromium steel wire (~12 μm
248 in diameter; see **Fig 1C**). Prior to insertion, tetrodes were coated with DiI to allow
249 anatomical tracing of the electrode path (**Fig 2A**). The tetrode array was lowered in ~100
250 μm increments until the tip reached Area X at ~3100 μm (right hemisphere) and allowed
251 to stabilize for 5-10 minutes prior to recording. Neural data was acquired at 20 kHz using
252 the INTAN neural recording system (Intan Technologies, Inc.). Neural recordings from
253 Area X neurons occurred in 5-minute blocks. After each 5-min block of data was acquired,
254 the electrode array was lowered ~50 μm and another recording block was acquired. All
255 recordings were restricted to Area X (3100-4100 μm). Data was spike sorted using
256 Kilosort v2.5 (https://zenodo.org/records/4482749) (71) and Phy
257 (https://github.com/cortex-lab/phy). Methods for cell-type estimation are described in
258 Results.

259 **Data/Statistical Analysis:**

260 All single-unit data was analyzed using Matlab (R2025a). All Matlab analysis code is
261 available upon publication at: https://github.com/CowenLab/ZebraFinch.

262 **Measurement of burst activity:** The temporal structure of the firing activity of individual
263 neurons was quantified using “local variance” (LV), a measure that assesses the

variability of inter-spike intervals (ISIs) and is robust to changes in firing rate (72). LV is computed from the vector of ISIs for each neuron as shown in the formula below:

$$LV = \frac{3}{n-1}\sum_{i=1}^{n-1}\left(1 + \frac{4I_iI_{i+1}}{(I_i+I_{i+1})^2}\right)\left(1 - \frac{4R}{I_i+I_{i+1}}\right), \qquad (1)$$

where I_i and I_{i+1} are the i-th and $i+1$ ISI and n is the number of ISIs. LV scores ~0 indicate tonic firing, scores ~1 show Poisson firing, and scores >1 indicate burst-like firing patterns.

Parametric and non-parametric tests were used for hypothesis testing. For group-level analysis of firing-rate data (n = 201 categorized neurons from n = 12 finches) non-parametric tests were used as firing rates do not follow normal distributions (73). Consequently, rank-sum tests were used for two-group comparisons and the Kruskal-Wallis test was used for multi-group data. The Holm-Bonferroni correction was used to correct for multiple comparisons. For normally distributed data, ANOVA and t-tests were used followed by Tukey or Holm-Bonferroni post-hoc corrections. Alpha was set to 0.05. Relationships between neural data and each bird's song features (e.g., mean Entropy, Duration, and Amplitude) were investigated using a generalized linear regression model where the outcome variable was neural activity (e.g., firing rate) and the independent variables were song features and group category (ASYN or GFP) as described in **Results and S2 Fig**. Multicollinearity between independent variables can impair the ability to interpret regression models. We observed that some song features did indeed covary (r > 0.4 for 5 song feature pairs). To address this, we repeated the regression using the first three principal components of the independent variable matrix and compared results to those from the original regression model. As reported in **S2 Fig**, similar results were obtained from the original and dimensionality-reduced model.

287

288 ## 2.4 Tissue processing and immunohistochemistry

289 Immediately following the end of the neural recording session, finches were humanely
290 euthanized by isoflurane inhalant overdose and transcardially perfused with warmed
291 saline followed by chilled 4% paraformaldehyde in Dulbecco's Phosphate Buffer Saline.
292 Fixed brains were cryoprotected in 20% sucrose overnight then cryosectioned in the
293 coronal plane at 30 µm on a Microtome cryostat through Area X. Tissue was processed,
294 following our previously published methods (45, 46) and summarized here: Hydrophobic
295 borders were drawn on the slides, using a pap pen (ImmEdge, Vector Labs) followed by
296 3 X 5 minute washes in TBS with 0.3% Triton X (Tx). To block non-specific antibody
297 binding, the tissue was then incubated for one hour at room temperature with 5% goat
298 serum (Sigma #G-9023) in TBS/0.3% Tx then 3 x 5-minute washes in 1% goat serum in
299 TBS/0.3% Tx were performed. A primary antibody was used against a-syn (1:250, rabbit,
300 Proteintech 10842-1-AP, RRID: AB_2192672). GFP expression was robust enough to be
301 visualized without an antibody.

302

303 The primary antibody was incubated in a solution of 1% goat serum in TBS/0.3% Tx
304 overnight at 4°C. One tissue section per slide was used as a 'no primary' control and a
305 pre-absorption control experiment was performed to validate antibody specificity in a
306 companion study evaluating the distribution of a-syn protein following AAV injection (46).
307 The next day, sections were washed 5 x 5 minutes in TBS/0.3% Tx and incubated for
308 three hrs at room temperature in a fluorescently conjugated secondary antibody (1:1000:
309 goat anti-rabbit 647 A-21245, RRID:AB_2535813). After secondary incubation, sections

310 were washed 3 x 10 minutes in TBS followed by 2 x 5 washes in filtered TBS. Slides were
311 then cover-slipped in Pro-Long Anti-Fade Gold mounting medium (Molecular Probes,
312 P36930) and imaged using a Zeiss Axio Observer 7 with Apotome III Microscope under
313 the University of Arizona Imaging Cores - Optical Core Facility (RRID:SCR_023355).

314

315 Results:

316 Virally-driven expression is confirmed in song nucleus Area X

317 **Fig 2** is a representative example of AAV expression in Area X. Two months post-virus
318 injection, we detected GFP cell bodies in Area X (**Fig 2A,C**) accompanied by low a-syn
319 protein expression (**Fig 2B**). By contrast, a finch overexpressing a-syn showed staining
320 in processes and cell bodies (**Fig 1D**). These results are consistent with our two prior
321 publications (45, 46).

322

323

324 **Fig 2. AAV expression in finch song nucleus Area X.** The Area X region is represented
325 by the dotted line. Small arrowheads denote the border between the striatum and the
326 nidopallium. Staining for alpha-synuclein (a-syn) protein is shown in red. **A)** An AAV
327 control expressing finch has GFP labeled cell bodies (green) in Area X and large
328 arrowhead denotes the last recorded tetrode position (yellow). **B)** A-syn protein
329 expression is low in Area X compared to surrounding basal ganglia in this AAV-GFP finch.
330 **C)** View of (A) showing the GFP channel only. **D)** An AAV-h*SNCA* expressing finch shows
331 widespread expression of a-syn in processes throughout Area X. Inset in bottom left

332 corner shows a zoomed in view of bead-like a-syn protein in the processes (inset scale
333 bar = 10 μm).
334

335 Extracellular identification of neuronal subtypes in anesthetized
336 finches

337 Area X neurons share much in common with neurons in the mammalian striatum
338 and pallidum. For example, the most abundant Area X neuron type is homologous to the
339 mammalian medium spiny neuron (MSN,(58)), with Area X and mammalian MSNs
340 sharing wide waveforms, low firing rates, and bursting activity (74-76). There is also
341 evidence that Area X contains striatal fast-firing interneurons, cholinergic interneurons,
342 and low-threshold spiking neurons (48, 74, 77). Furthermore, Area X contains two classes
343 of fast-firing pallidal-like neurons: local-circuit (HF-1) and thalamus-projecting (HF-2) (59,
344 78). These six cell classes were identified by their firing rates and waveform features
345 using multiple approaches from this literature, including correlating neuronal activity *in*
346 *vivo* with birdsong and patch-clamp recording in brain slices. Our present study is
347 constrained by the fact that all data was acquired from extracellular electrodes implanted
348 in anesthetized finches. We found no prior publications with recordings from Area X of
349 adult anesthetized finches; prior work includes some anesthetized recordings from lMAN
350 and Area X in the context of juvenile song learning (79). Consequently, our classification
351 was informed by criteria developed from *in vivo* recordings from Area X in singing finches
352 and restricted to waveform shape, firing rate, and assessment of bursting activity in the
353 following five identified categories (74, 78, 80).
354 Neuron categorization and criteria (results shown in **Fig 3**):

355 1) **Wide-Low-Rate (WLR) Criteria**: Neurons firing ≤ 6 Hz with a peak half width > 0.25
356 ms or a peak-to-trough width of > 0.35 ms (**Fig 3 A,D,E**). WLR neurons were also
357 more 'bursty'' relative to other neuronal types (**Fig 3F**) as measured by Local Variance
358 (LV, see Methods (81)) and were the most abundant of the five identified cell types
359 (**Fig 3C**). Together, these features suggest that WLR cells were MSN-like given
360 evidence that MSNs are the most prominent cell type in the striatum, exhibit wide
361 waveforms, have low firing rates, and express bursting activity (74) (75, 76).
362 2) **Wide-High-Rate (WHR) Criteria**: Neurons with a firing rate between 20 and 50 Hz
363 with a peak half width > 0.25 ms or a peak-to-trough width of > 0.35 ms (**Fig 3A,D,E**).
364 Post-classification analysis also showed that these neurons fired tonically (LV < 1, see
365 **Fig 3F**). Tonically active WHR cells have features consistent with striatal cholinergic
366 interneurons (74).
367 3) **Narrow-Low-Rate (NLR) Criteria**: Narrow waveform neurons firing ≤ 6 Hz (74) having
368 a peak half width < 0.25 ms or a peak-to-trough width of < 0.35 ms (**Fig 3A,D,E**).
369 4) **Narrow-High-Rate (NHR) Criteria**: Narrow waveform neurons with rates ≥ 8 Hz but
370 < 50Hz (**Fig 3A,D,E**). Narrow waveforms are characteristic of local circuit fast-firing
371 inhibitory neurons.
372 5) **Very-High-Rate (VHR) Criteria**: Neurons firing ≥ 50 Hz (**Fig 3A,D,E**). Area X pallidal-
373 like projection neurons are characterized by exceedingly high firing rates (74, 78).
374 Consequently, we established a category for neurons with rates ≥ 50 Hz. Waveform
375 features were not used to further subdivide neurons in this group given its small size
376 (n = 18 neurons, **Fig 3C**). Analysis of VHR firing activity revealed that these neurons
377 exhibited decidedly tonic activity, with a mean LV of 0.51 (**Fig 3F**). These data suggest

378 that the identified VHR neurons are type-2 pallidal-like projection neurons (HF-2 in
379 (78) (82)) given the presence of tonic firing and relatively wide waveforms.
380 Furthermore, the small size of this group is consistent with other reports that suggest
381 PAL neurons comprise approximately just 5.4% of the Area X cell population (58).
382
383 **Fig 3. Identification of five classes of Area X neurons in anesthetized finches. A)**
384 Mean shape for each of the five identified classes of neurons (n = 201 neurons from n =
385 12 finches). Neurons were categorized based on spike width and firing rate (see Results).
386 Amplitude is normalized such that the minimum (trough) = -1. Colors indicate neuron
387 subtype (see key). **B)** Inter-spike interval distributions for each neuronal subtype. Y-axis
388 indicates probability (p). **C)** Histogram indicating the number of identified neurons in each
389 category. **D)** Box plot of the half-width (ms-milliseconds) for each neuronal group. Each
390 dot indicates an individual neuron. Horizontal red lines indicate the median. Hypothesis
391 tests were not performed as half-width was a key criterion for classification. **E)** Firing rates
392 for each neuronal group (H-Hertz). Each dot indicates an individual neuron. Hypothesis
393 tests were not performed as firing rate was a key criterion for classification. **F)** Burst firing
394 differed between groups. While neurons were not categorized based on burst-firing, the
395 measure of bursting (Local Variance-LV) indicated that Wide-Low-Rate neurons had
396 increased burst firing (LV>1) relative to other groups (ANOVA $p < 0.000001$, Tukey post-
397 hoc comparison. Thick red lines indicate significant post-hoc differences (*$p < 0.05$, **$p <$
398 0.01 (not shown), ***$p < 0.001$). The red lines in the box plots indicate the median and the
399 whiskers indicate 1.5X the Interquartile Range.
400

401

402 ## Reduced Area X firing rates in ASYN overexpressing finches

403 We predicted that a-syn expression would reduce putative MSN (WLR) neuron
404 activity, thus releasing putative PAL neurons (VHR) from inhibition. Consequently, we
405 investigated whether firing rates of WLR neurons were reduced in the ASYN group and
406 whether rates in VHR neurons were increased. Visual inspection of raster plots of WLR
407 activity (**Fig 4A-B**) suggested reduced WLR firing activity in the ASYN group. Statistical
408 comparison of firing rates of GFP and ASYN neurons identified a significant difference
409 (**Fig 4C**, rank-sum, p = 0.005 before correction and p = 0.026 after Holm-Bonferroni
410 correction). No significant between-group differences were identified in the other neuronal
411 classes, including the VHR neurons.

412

413 **Fig 4. Reduced firing rates of WLR neurons in the ASYN group. A-B)** Raster plots of
414 WLR in the GFP and AAV-h*SNCA* (ASYN) groups. The x-axis shows time in seconds.
415 Each row is a raster for a distinct neuron. **C)** Between-group comparison (GFP vs. ASYN)
416 for each of the five neuron types. WLR neurons were only found in 4/6 finches. Firing
417 rates for WLR neurons were lower in the ASYN group relative to the GFP control (rank-
418 sum test, p = 0.005 prior to correction, *p = 0.026 after Holm-Bonferroni correction).

419

420 ## Burst firing was not changed in ASYN overexpressing finches

421 While burst firing is a canonical property of MSNs, MSN burst firing may become
422 dysregulated in PD. Indeed, altered MSN burst firing has been reported in the 6-OHDA
423 mouse model of PD (83), non-human MPTP primate models (84), and in human PD

424 patients (64). Consequently, we predicted that burst firing will be affected by ASYN
425 overexpression in finch Area X. To investigate this, the local variance (LV) measure (72),
426 see Methods) was used to evaluate the pattern of inter-spike intervals and quantify the
427 degree that neuronal activity was either tonic (low LV), Poisson (LV near 1), or bursty (LV
428 > 1). Contrary to our prediction, analysis of spiking statistics with LV did not identify any
429 difference between GFP and ASYN groups in LV values for any neuronal subtype (**Fig 5**,
430 t-test, all $p > 0.05$ after Holm-Bonferroni post-hoc correction). Thus, while ASYN
431 significantly reduced firing rates of WLR neurons, these changes were not accompanied
432 by a change in burst-firing.
433
434
435
436 **Fig 5. Local Variance (LV), a measure of bursting, is not different between ASYN**
437 **and GFP control groups.** Between-group comparisons (GFP vs. ASYN) were made for
438 each of the five neuron types, and no between-group differences were identified in any of
439 the neuron classes (rank-sum test, all $p > 0.05$ after Holm-Bonferroni post-hoc correction).
440

441 ## Extracellular waveform shape was altered in wide-waveform neurons

442 While waveform features and firing rates are commonly used to classify neurons
443 into putative subtypes (74, 80, 85), inferring physiological properties of neurons from
444 extracellular recordings is highly problematic as waveform features vary as a function of
445 recording location relative to the morphology of the neuron (86-88). Even so, we did
446 observe consistent differences in extracellular waveform shapes between ASYN and GFP
447 animals that encourage future investigations. Specifically, we found that WLR and WHR

448 neurons showed a large positive extracellular 'rebound' following the initial trough (**Fig**
449 **6A**). This was determined by first normalizing the waveform of each neuron such that the
450 trough = -1 and baseline was zero. Consequently, positive values indicate proportional
451 changes above baseline. The "Rebound Peak" for each neuron was measured as the
452 normalized amplitude of the largest peak following the time of the trough (t = 0 ms). Values
453 for each neuron type are shown in **Fig 6B** for the GFP and ASYN groups. Rank-sum tests
454 were performed, and significant between-group differences were identified in the WLR
455 and WHR groups (p_{WLR} = 0.003, p_{WHR} = 0.0002 after Bonferroni-Holm correction).
456
457
458 **Fig 6**. **ASYN group shows enhanced post-peak rebound for wide-waveform**
459 **neurons. A)** Mean waveforms for the ASYN and GFP groups for each neuron type. For
460 each waveform, data was normalized such that the distance from baseline to the trough
461 = -1. Inspection of these plots suggested that wide-waveform (WLR, WHR) ASYN
462 neurons had a larger rebound following the initial trough. **B)** Statistical analysis of the
463 rebound was performed by measuring the normalized amplitude of the largest peak
464 following t=0 (rebound peak) for each neuron (dots). These values were compared
465 between groups using rank-sum tests and p values were adjusted using the Holm-
466 Bonferroni correction. **p<0.01, ***p<0.001. Error bars in box plots indicate ±SEM.
467
468 **No observed correlation between song features and neuronal firing**
469 **properties**

470 Next, we investigated whether ASYN and GFP birds differed in their song features
471 and if variation in mean WLR neuronal activity in each bird correlated with song features.
472 Analysis of syllable-level features failed to identify any between-group difference (Mann-
473 Whitney U test, $p > 0.05$, **S1 Fig, S1 Table**).
474 Investigation of whether firing rates correlated with song features was performed
475 by first calculating the mean firing rate of WLR neurons (the largest group and the putative
476 MSNs) for each bird. Two birds had to be excluded from the analysis as no WLR neurons
477 were identified in these animals. Mean WLR firing rates were used as the outcome
478 variable for a generalized linear model where the independent variables were song
479 features (mean amplitude, duration, and entropy and CV amplitude, duration, and
480 entropy) and the group (ASYN or GFP). No significant relationship between song features
481 and firing rate was identified ($F(10,2) = 11.7$, $p = 0.082$);**S2 Fig**.
482
483

484 # 4. Discussion

485 The goal of this study was to obtain new information about the cellular and network-
486 level activity affected by overexpression of human a-syn protein in an adult male zebra
487 finch model. To carry out this goal, we performed extracellular recordings from song
488 nucleus Area X of the basal ganglia in anesthetized adult male finches and identified five
489 distinct cell types. Our main finding was that wide, low firing rate (WLR) neurons, putative
490 MSNs, show reduced firing activity and enhanced post-inhibitory rebound in the a-syn
491 overexpression condition compared to controls. This aligns with our working hypothesis
492 that abnormally elevated a-syn protein levels in Area X will decrease MSNs firing rate.

493 We also predicted that GP-projecting neurons would show reduced firing in Area X. VHR
494 neurons may represent these GP-projecting neurons, but they did not show a difference
495 in firing rate between the ASYN and GFP control groups. This finding may reflect low
496 statistical power given the small number of VHR neurons recorded.
497
498 A benefit of anesthetized recordings is that they allow for high data throughput,
499 enabling the recording of a substantial proportion of neurons without confounds due to
500 animal movement. A limitation of this approach in our finch model is that on-going real
501 time modification of neural activity related to song production cannot be evaluated. It is
502 also likely that neuronal activity was dampened by isoflurane anesthesia. While
503 information is scarce on the effects of isoflurane on *in vivo* recordings from the striatum
504 of naïve finches or rodents, patch clamp studies in rat brain slices show that brief
505 isoflurane exposure can dampen sodium currents in hippocampal neurons (89) and
506 reduce spiking and bursting modes in thalamic neurons (90). Our future investigations will
507 compare isoflurane-induced anesthesia on Area X of naïve finches versus awake, singing
508 finches where we can examine how a-syn modulates neuronal dynamics under more
509 physiologically relevant conditions.
510 The observed reduction in WLR (putative MSN) firing rates observed in Area X of
511 the ASYN finches contrasts with some measures of MSN activity reported in human PD
512 patients and primate PD models. For example, striatal projection neurons in the human
513 basal ganglia of PD patients undergoing deep brain stimulation had high frequency
514 neuronal firing patterns resembling the advanced parkinsonism of the Non-Human
515 Primate model, with hyperactivity and “bursty” neuronal firing activity (14, 64). In a mouse

516 model of bilateral dopamine depletion (via the neurotoxin 6-OHDA) in the dorsolateral
517 striatum, single unit recordings from MSNs showed reduced bursting activity during
518 movement. Intriguingly, they classified MSNs into two types with type 1 showing
519 increased firing during movement and type 2, decreased firing with no difference in firing
520 rate when the mouse was stationary (83). In freely moving rats, 6-OHDA treatment
521 increased oscillatory synchronization in the striatum (91). Future recordings in singing,
522 ambulatory finches with the ASYN phenotype will determine if hyperactivity of MSNs and
523 differential sub-types exist, evidence for dopamine loss, and how these various sub-
524 components contribute to changes in real-time song output.
525
526 The reduced firing rates of WLR neurons in ASYN expressing finches may reflect
527 reduced mean frequency of spontaneous excitatory postsynaptic glutamatergic currents
528 (EPSCs) from cortical song nucleus lMAN onto Area X MSNs and GP neurons. Striatal
529 recordings from h*SNCA* overexpressing mice show reduced glu currents (12). Future
530 work using electrophysiological recordings from Area X brain slices *in vitro* can determine
531 whether glu input is perturbed in our ASYN condition.
532 ASYN-driven abnormal changes in synaptic input to Area X may also be
533 accompanied by altered intrinsic membrane properties. Both the WLR and WHR neuronal
534 classes showed greater positive rebound potential following the initial spike in the ASYN
535 expressing group compared to GFP controls. While extracellular recordings of action
536 potentials cannot reliably identify after-hyperpolarization (AHP) currents, the observed
537 rebound potential occurs during the typical time interval of the AHP, suggesting that
538 membrane properties in the ASYN neurons are altered. The AHP is regulated by K^+

539 currents, and several classes of K^+ channels are implicated in altered neuronal excitability
540 in PD models (92). The significantly larger rebound potential in the ASYN expressing
541 group may reflect an enhanced AHP-related conductance. Patch-clamp
542 electrophysiology in brain slices is a necessary approach to confirm true fluctuations in
543 membrane properties during the AHP period. Changes in AHP-related conductance could
544 result from increased SK/BK channel activity (93) (94)) or a reduction in I_h current (95,
545 96), leading to greater hyperpolarization following spikes and dampened excitability. In
546 nigral DA neurons, abnormal a-syn oligo aggregates increase the conductance of K^+_{ATP}
547 channels leading to reduced firing (97). In our finch model, a-syn overexpression could
548 progressively decrease intrinsic excitability in MSNs via these channels, and/or others.
549 To evaluate the specific role of a-syn expression on MSNs, future directions will employ
550 a custom-made AAV containing a CAMKII promoter that has been previously used in
551 naïve finches to evaluate MSNs firing activity (98). By selectively overexpressing a-syn in
552 MSNs, we can evaluate the relationship between the extent of protein pathology and the
553 neural activity changes underlying song. In a recent publication, we found that regional
554 changes in virally-expressed human a-syn protein within Area X correlated with changes
555 in syllable level features. For example, we detected a positive correlation between right
556 hemisphere a-syn proteinopathy and a reduction in the variation of harmonic syllable
557 duration, among other features correlated to the right hemisphere Area X (46). Our neural
558 recordings here are also from right hemisphere Area X; the contribution of the left Area X
559 is not known. Prior studies suggest a transition between right-side dominance of song
560 nucleus HVC in adult birdsong (99) while the left-side dominates during juvenile
561 learning(100). Thus, when assessing cell-type changes in electrical activity within brain

nuclei aligned with real-time singing behavior, factors to take into account include the recording hemisphere, the distribution of protein expression, and the presence of pathology, e.g. a-syn aggregates in individual cell types.

Conclusions

Our study takes an important first step forward in evaluating the consequences of a-syn overexpression on the activities of neuronal subtypes involved in vocal behavior. A growing body of research has elucidated the role that neurons in the cortico-striatal-thalamic circuit play in male zebra finch song production. By introducing human a-syn to the zebra finch model, this study supports a systems- and cellular-level investigation of human vocal deficits in PD. This is important given that current medications and brain stimulation used in the treatment of PD fail to resolve the vocal deficits and can worsen them (101-103). Data from pre-clinical animal models such as the songbird can provide important mechanistic insight needed for the development of new brain-targeted cellular therapies for the vocal dysfunction.

CRediT Contributions

CRediT authorship contribution statement: Brian R. Dominguez: Data curation, Investigation, Methodology, Validation, Visualization, Writing-Original Draft, Writing-review & editing. Gabriel Holguin: Data curation, Formal Analysis, Investigation, Methodology, Software, Validation, Visualization, Writing-Original Draft, Writing-review & editing. Madeleine S. Daly: Data curation, Formal Analysis, Investigation, Methodology,

586 Validation, Writing-review & editing. Reed T. Bjork: Investigation, Methodology,
587 Validation, Visualization, Writing-review & editing. Stephen Cowen: Conceptualization,
588 Data Curation, Formal Analysis, Investigation, Methodology, Software, Supervision,
589 Validation, Visualization, Writing-Original Draft, Writing-review & editing. Julie E. Miller:
590 Conceptualization, Data curation, Formal Analysis, Funding acquisition, Investigation,
591 Methodology, Project administration, Resources, Supervision, Validation, Visualization,
592 Writing-original draft, Writing-review & editing.
593
594

595

596 # Acknowledgements

597 We thank Kathy Dillon, Michelle Gordon, and Mauricio Serna for technical contributions
598 along with University of Arizona Animal Care staff and Mr. Douglas Cromey of the
599 University of Arizona Imaging Cores - Optical Core Facility (RRID:SCR_023355).
600
601

602 # References

603 1. Polymeropoulos MH, Lavedan C, Leroy E, Ide SE, Dehejia A, Dutra A, et al.
604 Mutation in the alpha-synuclein gene identified in families with Parkinson's disease.
605 Science. 1997;276(5321):2045-7.

606 2. Chartier-Harlin M-C, Kachergus J, Roumier C, Mouroux V, Douay X, Lincoln S, et
607 al. α-synuclein locus duplication as a cause of familial Parkinson's disease. The Lancet.
608 2004;364(9440):1167-9.
609 3. Singleton A, Farrer M, Johnson J, Singleton A, Hague S, Kachergus J, et al. α-
610 Synuclein locus triplication causes Parkinson's disease. Science. 2003;302(5646):841-.
611 4. Mak E, Su L, Williams GB, O'Brien JT. Neuroimaging characteristics of dementia
612 with Lewy bodies. Alzheimer's research & therapy. 2014;6:1-10.
613 5. Koga S, Dickson DW. Recent advances in neuropathology, biomarkers and
614 therapeutic approach of multiple system atrophy. Journal of Neurology, Neurosurgery &
615 Psychiatry. 2018;89(2):175-84.
616 6. Calo L, Wegrzynowicz M, Santivanez-Perez J, Grazia Spillantini M. Synaptic
617 failure and alpha-synuclein. Movement disorders: official journal of the Movement
618 Disorder Society. 2016;31(2):169-77.
619 7. Marino G, Calabresi P, Ghiglieri V. Alpha-synuclein and cortico-striatal plasticity in
620 animal models of Parkinson disease. Handbook of clinical neurology. 2022;184:153-66.
621 8. Calabresi P, Mechelli A, Natale G, Volpicelli-Daley L, Di Lazzaro G, Ghiglieri V.
622 Alpha-synuclein in Parkinson's disease and other synucleinopathies: from overt
623 neurodegeneration back to early synaptic dysfunction. Cell death & disease.
624 2023;14(3):176.
625 9. Watson JB, Hatami A, David H, Masliah E, Roberts K, Evans CE, et al. Alterations
626 in corticostriatal synaptic plasticity in mice overexpressing human alpha-synuclein.
627 Neuroscience. 2009;159(2):501-13.

628 10. Tozzi A, de Iure A, Bagetta V, Tantucci M, Durante V, Quiroga-Varela A, et al.
629 Alpha-Synuclein Produces Early Behavioral Alterations via Striatal Cholinergic Synaptic
630 Dysfunction by Interacting With GluN2D N-Methyl-D-Aspartate Receptor Subunit. Biol
631 Psychiat. 2016;79(5):402-14.
632 11. Tozzi A, Sciaccaluga M, Loffredo V, Megaro A, Ledonne A, Cardinale A, et al.
633 Dopamine-dependent early synaptic and motor dysfunctions induced by α-synuclein in
634 the nigrostriatal circuit. Brain. 2021;144(11):3477-91.
635 12. Wu N, Joshi PR, Cepeda C, Masliah E, Levine MS. Alpha-synuclein
636 overexpression in mice alters synaptic communication in the corticostriatal pathway.
637 Journal of neuroscience research. 2010;88(8):1764-76.
638 13. Lam HA, Wu N, Cely I, Kelly RL, Hean S, Richter F, et al. Elevated tonic
639 extracellular dopamine concentration and altered dopamine modulation of synaptic
640 activity precede dopamine loss in the striatum of mice overexpressing human α-synuclein.
641 Journal of neuroscience research. 2011;89(7):1091-102.
642 14. Beck G, Singh A, Papa SM. Dysregulation of striatal projection neurons in
643 Parkinson's disease. Journal of Neural Transmission. 2018;125(3):449-60.
644 15. Durante V, de Iure A, Loffredo V, Vaikath N, De Risi M, Paciotti S, et al. Alpha-
645 synuclein targets GluN2A NMDA receptor subunit causing striatal synaptic dysfunction
646 and visuospatial memory alteration. Brain. 2019;142(5):1365-85.
647 16. Wilson CJ, Groves PM. Spontaneous firing patterns of identified spiny neurons in
648 the rat neostriatum. Brain research. 1981;220(1):67-80.
649 17. Kita H, Kita T. Role of striatum in the pause and burst generation in the globus
650 pallidus of 6-OHDA-treated rats. Frontiers in systems neuroscience. 2011;5:42.

651 18. Henkel LM, Kankowski S, Moellenkamp TM, Smandzich NJ, Schwarz S, Di Fonzo
652 A, et al. iPSC-derived striatal medium spiny neurons from patients with multiple system
653 atrophy show hypoexcitability and elevated α-synuclein release. Cells. 2023;12(2):223.
654 19. Lobb CJ, Zaheer AK, Smith Y, Jaeger D. In vivo electrophysiology of nigral and
655 thalamic neurons in alpha-synuclein-overexpressing mice highlights differences from
656 toxin-based models of parkinsonism. Journal of neurophysiology. 2013;110(12):2792-
657 805.
658 20. Brys I, Nunes J, Fuentes R. Motor deficits and beta oscillations are dissociable in
659 an alpha-synuclein model of Parkinson's disease. European Journal of Neuroscience.
660 2017;46(3):1906-17.
661 21. Robson E, Tweedy C, Manzanza N, Taylor J-P, Atkinson P, Randall F, et al.
662 Impaired fast network oscillations and mitochondrial dysfunction in a mouse model of
663 alpha-synucleinopathy (A30P). Neuroscience. 2018;377:161-73.
664 22. Sapir S. Multiple factors are involved in the dysarthria associated with Parkinson's
665 disease: a review with implications for clinical practice and research. Journal of speech,
666 language, and hearing research : JSLHR. 2014;57(4):1330-43.
667 23. Ma A, Lau KK, Thyagarajan D. Voice changes in Parkinson’s disease: What are
668 they telling us? Journal of Clinical Neuroscience. 2020;72:1-7.
669 24. Stewart C, Winfield L, Hunt A, Bressman SB, Fahn S, Blitzer A, et al. Speech
670 dysfunction in early Parkinson's disease. Movement disorders: official journal of the
671 Movement Disorder Society. 1995;10(5):562-5.
672 25. Ho AK, Iansek R, Marigliani C, Bradshaw JL, Gates S. Speech impairment in a
673 large sample of patients with Parkinson's disease. Behav Neurol. 1998;11(3):131-7.

26. Harel B, Cannizzaro M, Snyder PJ. Variability in fundamental frequency during speech in prodromal and incipient Parkinson's disease: a longitudinal case study. Brain Cogn. 2004;56(1):24-9.

27. Skodda S, Schlegel U. Speech rate and rhythm in Parkinson's disease. Movement disorders: official journal of the Movement Disorder Society. 2008;23(7):985-92.

28. Skodda S, Rinsche H, Schlegel U. Progression of dysprosody in Parkinson's disease over time--a longitudinal study. Movement disorders: official journal of the Movement Disorder Society. 2009;24(5):716-22.

29. Rusz J, Cmejla R, Ruzickova H, Ruzicka E. Quantitative acoustic measurements for characterization of speech and voice disorders in early untreated Parkinson's disease. The Journal of the Acoustical Society of America. 2011;129(1):350-67.

30. Defazio G, Guerrieri M, Liuzzi D, Gigante AF, di Nicola V. Assessment of voice and speech symptoms in early Parkinson's disease by the Robertson dysarthria profile. Neurol Sci. 2016;37(3):443-9.

31. V. Berisha JL, T. Huston, A. Wisler, Y. Jiao, and J. Eig. Float Like a Butterfly Sting Like a Bee: Changes in Speech Preceded Parkinsonism Diagnosis for Muhammad Ali. Proceedings of the 2017 Interspeech Conference.

32. Rusz J, Tykalová T, Novotný M, Růžička E, Dušek P. Distinct patterns of speech disorder in early-onset and late-onset de-novo Parkinson’s disease. npj Parkinson's Disease. 2021;7(1):98.

33. Šimek M, Rusz J. Validation of cepstral peak prominence in assessing early voice changes of Parkinson's disease: Effect of speaking task and ambient noise. The Journal of the Acoustical Society of America. 2021;150(6):4522-33.

697 34. Berus L, Klancnik S, Brezocnik M, Ficko M. Classifying Parkinson's disease based
698 on acoustic measures using artificial neural networks. Sensors. 2018;19(1):16.
699 35. Solana-Lavalle G, Galán-Hernández J-C, Rosas-Romero R. Automatic Parkinson
700 disease detection at early stages as a pre-diagnosis tool by using classifiers and a small
701 set of vocal features. Biocybernetics and Biomedical Engineering. 2020;40(1):505-16.
702 36. Suppa A, Costantini G, Asci F, Di Leo P, Al-Wardat MS, Di Lazzaro G, et al. Voice
703 in Parkinson's disease: a machine learning study. Frontiers in Neurology.
704 2022;13:831428.
705 37. Lim WS, Chiu S-I, Wu M-C, Tsai S-F, Wang P-H, Lin K-P, et al. An integrated
706 biometric voice and facial features for early detection of Parkinson's disease. npj
707 Parkinson's Disease. 2022;8(1):145.
708 38. Ciucci MR, Ma ST, Fox C, Kane JR, Ramig LO, Schallert T. Qualitative changes
709 in ultrasonic vocalization in rats after unilateral dopamine depletion or haloperidol: a
710 preliminary study. Behav Brain Res. 2007;182(2):284-9.
711 39. Gombash SE, Manfredsson FP, Kemp CJ, Kuhn NC, Fleming SM, Egan AE, et al.
712 Morphological and behavioral impact of AAV2/5-mediated overexpression of human
713 wildtype alpha-synuclein in the rat nigrostriatal system. PloS one. 2013;8(11):e81426.
714 40. Miller JE, Hafzalla GW, Burkett ZD, Fox CM, White SA. Reduced vocal variability
715 in a zebra finch model of dopamine depletion: implications for Parkinson disease. Physiol
716 Rep. 2015;3(11).
717 41. Grant LM, Kelm-Nelson CA, Hilby BL, Blue KV, Paul Rajamanickam ES, Pultorak
718 JD, et al. Evidence for early and progressive ultrasonic vocalization and oromotor deficits

719 in a PINK1 gene knockout rat model of Parkinson's disease. J Neurosci Res.
720 2015;3:1713–27.
721 42. Yang KM, Blue KV, Mulholland HM, Kurup MP, Kelm-Nelson CA, Ciucci MR.
722 Characterization of oromotor and limb motor dysfunction in the DJ1-/-model of Parkinson
723 disease. Behavioural brain research. 2018;339:47-56.
724 43. Kelm-Nelson CA, Gammie S. Gene expression within the periaqueductal gray is
725 linked to vocal behavior and early-onset parkinsonism in Pink1 knockout rats. BMC
726 genomics. 2020;21:1-13.
727 44. Grant LM, Richter F, Miller JE, White SA, Fox CM, Zhu C, et al. Vocalization deficits
728 in mice over-expressing alpha-synuclein, a model of pre-manifest Parkinson's disease.
729 Behavioral neuroscience. 2014;128(2):110-21.
730 45. Medina CA, Vargas E, Munger SJ, Miller JE. Vocal changes in a zebra finch model
731 of Parkinson's disease characterized by alpha-synuclein overexpression in the song-
732 dedicated anterior forebrain pathway. PloS one. 2022;17(5):e0265604.
733 46. Bjork RT, Patel FZ, Daly MS, Miller JE. Evaluating alpha-synuclein proteinopathy
734 and consequences for birdsong in zebra finch basal ganglia Area X. Behavioural Brain
735 Research. 2025:115698.
736 47. Brainard MS, Doupe AJ. Translating birdsong: songbirds as a model for basic and
737 applied medical research. Annu Rev Neurosci. 2013;36:489-517.
738 48. Farries MA, Perkel DJ. Electrophysiological properties of avian basal ganglia
739 neurons recorded in vitro. Journal of neurophysiology. 2000;84(5):2502-13.
740 49. Person AL, Gale SD, Farries MA, Perkel DJ. Organization of the songbird basal
741 ganglia, including area X. J Comp Neurol. 2008;508(5):840-66.

742 50. Gale SD, Perkel DJ. Anatomy of a songbird basal ganglia circuit essential for vocal
743 learning and plasticity. Journal of chemical neuroanatomy. 2010;39(2):124-31.
744 51. Reiner A, Perkel DJ, Bruce L, Butler AB, Csillag A, Kuenzel W, et al. Revised
745 nomenclature for avian telencephalon and some related brainstem nuclei. *Journal of*
746 *Comparative Neurology*. 2004;473:377-414.
747 52. White SA. Genes and vocal learning. Brain Lang. 2010;115(1):21-8.
748 53. Simonyan K, Horwitz B, Jarvis ED. Dopamine regulation of human speech and bird
749 song: A critical review. Brain Lang. 2012;122(3):142-50.
750 54. Pfenning AR, Hara E, Whitney O, Rivas MV, Wang R, Roulhac PL, et al.
751 Convergent transcriptional specializations in the brains of humans and song-learning
752 birds. Science. 2014;346(6215):1256846.
753 55. Woolley SC, Kao MH. Variability in action: Contributions of a songbird cortical-
754 basal ganglia circuit to vocal motor learning and control. Neuroscience. 2015;296:39-47.
755 56. Lovell PV, Wirthlin M, Kaser T, Buckner AA, Carleton JB, Snider BR, et al. ZEBrA:
756 Zebra finch Expression Brain Atlas—A resource for comparative molecular
757 neuroanatomy and brain evolution studies. Journal of Comparative Neurology.
758 2020;528(12):2099-131.
759 57. Sakata JT, Birdsong D. Vocal Learning and Behaviors in Birds and Human
760 Bilinguals: Parallels, Divergences and Directions for Research. Languages. 2021;7(1):5.
761 58. Reiner A, Laverghetta AV, Meade CA, Cuthbertson SL, Bottjer SW. An
762 immunohistochemical and pathway tracing study of the striatopallidal organization of area
763 X in the male zebra finch. J Comp Neurol. 2004;469(2):239-61.

764 59. Farries MA, Perkel DJ. A telencephalic nucleus essential for song learning
765 contains neurons with physiological characteristics of both striatum and globus pallidus.
766 The Journal of neuroscience: the official journal of the Society for Neuroscience.
767 2002;22(9):3776-87.
768 60. Coleman MJ, Roy A, Wild JM, Mooney R. Thalamic gating of auditory responses
769 in telencephalic song control nuclei. Journal of Neuroscience. 2007;27(37):10024-36.
770 61. Peh WY, Roberts TF, Mooney R. Imaging auditory representations of song and
771 syllables in populations of sensorimotor neurons essential to vocal communication.
772 Journal of Neuroscience. 2015;35(14):5589-605.
773 62. Woolley SC, Rajan R, Joshua M, Doupe AJ. Emergence of context-dependent
774 variability across a basal ganglia network. Neuron. 2014;82(1):208-23.
775 63. Farries MA, Ding L, Perkel DJ. Evidence for "direct" and "indirect" pathways
776 through the song system basal ganglia. J Comp Neurol. 2005;484(1):93-104.
777 64. Singh A, Mewes K, Gross RE, DeLong MR, Obeso JA, Papa SM. Human striatal
778 recordings reveal abnormal discharge of projection neurons in Parkinson's disease.
779 Proceedings of the National Academy of Sciences. 2016;113(34):9629-34.
780 65. Kojima S, Kao MH, Doupe AJ. Task-related "cortical" bursting depends critically
781 on basal ganglia input and is linked to vocal plasticity. Proceedings of the National
782 Academy of Sciences of the United States of America. 2013;110(12):4756-61.
783 66. Moll FW, Kranz D, Corredera Asensio A, Elmaleh M, Ackert-Smith LA, Long MA.
784 Thalamus drives vocal onsets in the zebra finch courtship song. Nature. 2023:1-5.
785 67. Tchernichovski O, Nottebohm F, Ho CE, Pesaran B, Mitra PP. A procedure for an
786 automated measurement of song similarity. Animal Behaviour. 2000;59:1167-76.

68. Badwal A, Poertner J, Samlan RA, Miller JE. Common terminology and acoustic measures for human voice and birdsong. Journal of Speech, Language, and Hearing Research. 2018;61(12).

69. Badwal A, Borgstrom M, Samlan RA, Miller JE. Middle age, a key time point for changes in birdsong and human voice. Behavioral neuroscience. 2020;134(3):208.

70. Sober SJ, Wohlgemuth MJ, Brainard MS. Central contributions to acoustic variation in birdsong. The Journal of neuroscience: the official journal of the Society for Neuroscience. 2008;28(41):10370-9.

71. Pachitariu M, Steinmetz NA, Kadir SN, Carandini M, Harris KD. Fast and accurate spike sorting of high-channel count probes with KiloSort. Advances in neural information processing systems. 2016;29.

72. Shinomoto S, Kim H, Shimokawa T, Matsuno N, Funahashi S, Shima K, et al. Relating neuronal firing patterns to functional differentiation of cerebral cortex. PLoS computational biology. 2009;5(7):e1000433.

73. Buzsáki G, Mizuseki K. The log-dynamic brain: how skewed distributions affect network operations. Nature reviews neuroscience. 2014;15(4):264-78.

74. Goldberg JH, Fee MS. Singing-related neural activity distinguishes four classes of putative striatal neurons in the songbird basal ganglia. Journal of neurophysiology. 2010;103:2002-14.

75. Berke JD, Okatan M, Skurski J, Eichenbaum HB. Oscillatory entrainment of striatal neurons in freely moving rats. Neuron. 2004;43(6):883-96.

76. Wilson CJ. The generation of natural firing patterns in neostriatal neurons. Progress in brain research. 1993;99:277-97.

810 77. Budzillo A, Duffy A, Miller KE, Fairhall AL, Perkel DJ. Dopaminergic modulation of
811 basal ganglia output through coupled excitation-inhibition. Proceedings of the National
812 Academy of Sciences of the United States of America. 2017;114(22):5713-8.
813 78. Goldberg JH, Adler A, Bergman H, Fee MS. Singing-related neural activity
814 distinguishes two putative pallidal cell types in the songbird basal ganglia: comparison to
815 the primate internal and external pallidal segments. The Journal of neuroscience: the
816 official journal of the Society for Neuroscience. 2010;30(20):7088-98.
817 79. Doupe AJ, Solis MM, Kimpo R, Boettiger CA. Cellular, circuit, and synaptic
818 mechanisms in song learning. Annals of the New York Academy of Sciences.
819 2004;1016(1):495-523.
820 80. Barthó P, Hirase H, Monconduit L, Zugaro M, Harris KD, Buzsaki G.
821 Characterization of neocortical principal cells and interneurons by network interactions
822 and extracellular features. Journal of neurophysiology. 2004;92(1):600-8.
823 81. Shinomoto S, Shima K, Tanji J. Differences in spiking patterns among cortical
824 neurons. Neural computation. 2003;15(12):2823-42.
825 82. Bugaysen J, Bronfeld M, Tischler H, Bar-Gad I, Korngreen A. Electrophysiological
826 characteristics of globus pallidus neurons. PloS one. 2010;5(8):e12001.
827 83. Chen H, Lei H, Xu Q. Neuronal activity pattern defects in the striatum in awake
828 mouse model of Parkinson's disease. Behavioural brain research. 2018;341:135-45.
829 84. Singh A, Liang L, Kaneoke Y, Cao X, Papa SM. Dopamine regulates distinctively
830 the activity patterns of striatal output neurons in advanced parkinsonian primates. Journal
831 of neurophysiology. 2015;113(5):1533-44.

832 85. Vishwanath A, Bartlett MJ, Falk T, Cowen SL. Decoupling of motor cortex to
833 movement in Parkinson's dyskinesia rescued by sub-anaesthetic ketamine. Brain.
834 2025;148(6):2135-50.
835 86. Gold C, Henze DA, Koch C, Buzsaki G. On the origin of the extracellular action
836 potential waveform: a modeling study. Journal of neurophysiology. 2006;95(5):3113-28.
837 87. Teleńczuk M, Brette R, Destexhe A, Teleńczuk B. Contribution of the axon initial
838 segment to action potentials recorded extracellularly. Eneuro. 2018;5(3).
839 88. Bakkum DJ, Obien MEJ, Radivojevic M, Jäckel D, Frey U, Takahashi H, et al. The
840 axon initial segment is the dominant contributor to the neuron's extracellular electrical
841 potential landscape. Advanced biosystems. 2019;3(2):1800308.
842 89. Zhao W, Zhang M, Liu J, Liang P, Wang R, Hemmings HC, et al. Isoflurane
843 modulates hippocampal CA1 pyramidal neuron excitability by inhibition of both transient
844 and persistent sodium currents in mice. Anesthesiology. 2019;131(1):94.
845 90. Ries CR, Puil E. Isoflurane prevents transitions to tonic and burst firing modes in
846 thalamic neurons. Neuroscience letters. 1993;159(1-2):91-4.
847 91. Dejean C, Gross CE, Bioulac B, Boraud T. Dynamic changes in the cortex-basal
848 ganglia network after dopamine depletion in the rat. Journal of neurophysiology.
849 2008;100(1):385-96.
850 92. Choudhury SP, Bano S, Sen S, Suchal K, Kumar S, Nikolajeff F, et al. Altered
851 neural cell junctions and ion-channels leading to disrupted neuron communication in
852 Parkinson's disease. npj Parkinson's Disease. 2022;8(1):66.

853 93. Deister CA, Chan CS, Surmeier DJ, Wilson CJ. Calcium-activated SK channels
854 influence voltage-gated ion channels to determine the precision of firing in globus pallidus
855 neurons. Journal of Neuroscience. 2009;29(26):8452-61.
856 94. Faber EL, Sah P. Physiological role of calcium-activated potassium currents in the
857 rat lateral amygdala. Journal of Neuroscience. 2002;22(5):1618-28.
858 95. Robinson RB, Siegelbaum SA. Hyperpolarization-activated cation currents: from
859 molecules to physiological function. Annual review of physiology. 2003;65(1):453-80.
860 96. Storm JF. Potassium currents in hippocampal pyramidal cells. Progress in brain
861 research. 1990;83:161-87.
862 97. Hill E, Gowers R, Richardson M, Wall M. α-Synuclein aggregates increase the
863 conductance of substantia nigra dopamine neurons, an effect partly reversed by the
864 KATP channel inhibitor glibenclamide. eneuro. 2021;8(1).
865 98. Singh Alvarado J, Goffinet J, Michael V, Liberti W, Hatfield J, Gardner T, et al.
866 Neural dynamics underlying birdsong practice and performance. Nature. 2021:1-5.
867 99. Williams H, Crane LA, Hale TK, Esposito MA, Nottebohm F. Right-side dominance
868 for song control in the zebra finch. Journal of Neurobiology. 1992;23(8):1006-20.
869 100. Frank SY, Hunt JL, Bae AJ, Chirathivat N, Lotfi S, Raja SC, et al. Hemispheric
870 dominance in HVC is experience-dependent in juvenile male zebra finches. Scientific
871 reports. 2024;14(1):5781.
872 101. Plowman-Prine E, Okun M, Sapienza C, Shrivastav R, Fernandez H, Foote K, et
873 al. Perceptual characteristics of Parkinsonian speech: a comparison of the
874 pharmacological effects of levodopa across speech and non-speech motor systems.
875 NeuroRehabilitation. 2009;24(2):131-44.

102. Skodda S. Effect of deep brain stimulation on speech performance in Parkinson's disease. Parkinson's Disease. 2012;2012.

103. Fabbri M, Guimaraes I, Cardoso R, Coelho M, Guedes LC, Rosa MM, et al. Speech and voice response to a levodopa challenge in late-stage Parkinson's Disease. Front Neurol. 2017;8:432.

Supporting Information

S1 Table 1. Song data and statistics. For further information, see legends embedded into the tabs of this excel file.

S1 Fig. Exemplar song motif and group level comparisons of song syllable data. **A)** Spectrogram of song motif from a pre-injected GFP control bird (as in **Fig 2A-C**) with time in seconds on the x-axis and frequency in kilo (k) Hertz on the y-axis. Unique syllables are assigned a letter (A-E) and classified into harmonic, noisy, or mixed syllables (68). **B-E)** The mean and SEM scores shown for syllable level acoustic features (duration, amplitude, and entropy) for the ASYN (red) and GFP (black) control groups. Raw scores can be found in the **S1 Table**. The y-axis is the normalized score calculated from dividing the post-AAV injection scores by the pre-injection scores. Each dot represents an average score per finch. **B)** Comparisons of all syllable types combined or by individual syllable types **(C-E)** reveal no group differences (Mann Whitney U, $p>0.05$). Individual variation in CV scores is detected.

898 **S2 Fig. No significant correlation between song features and firing rate.** Scatter plots
899 showing the mean firing rate of WLR neurons averaged for each animal (dot) organized
900 by GFP (black) and ASYN (red) groups. Plots were generated for each song feature,
901 representing all syllable types combined. Generalized linear regression (see Results) did
902 not identify a relationship between firing rate and song features or group ($p = 0.0815$).
903

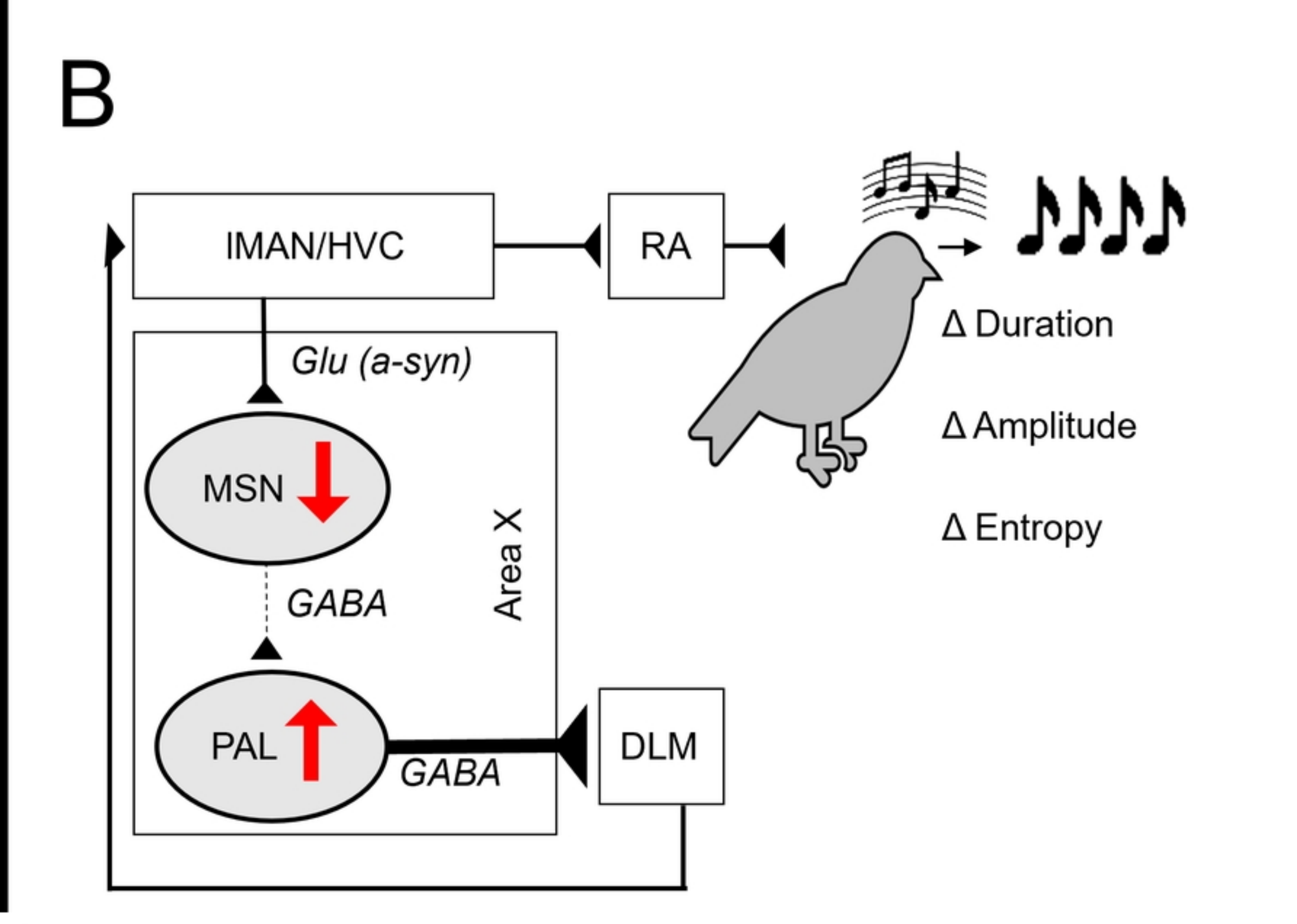
B
IMAN/HVC
RA
Glu (a-syn)
MSN
GABA
Area X
PAL
GABA
DLM
Δ Duration
Δ Amplitude
Δ Entropy

Figure 1B

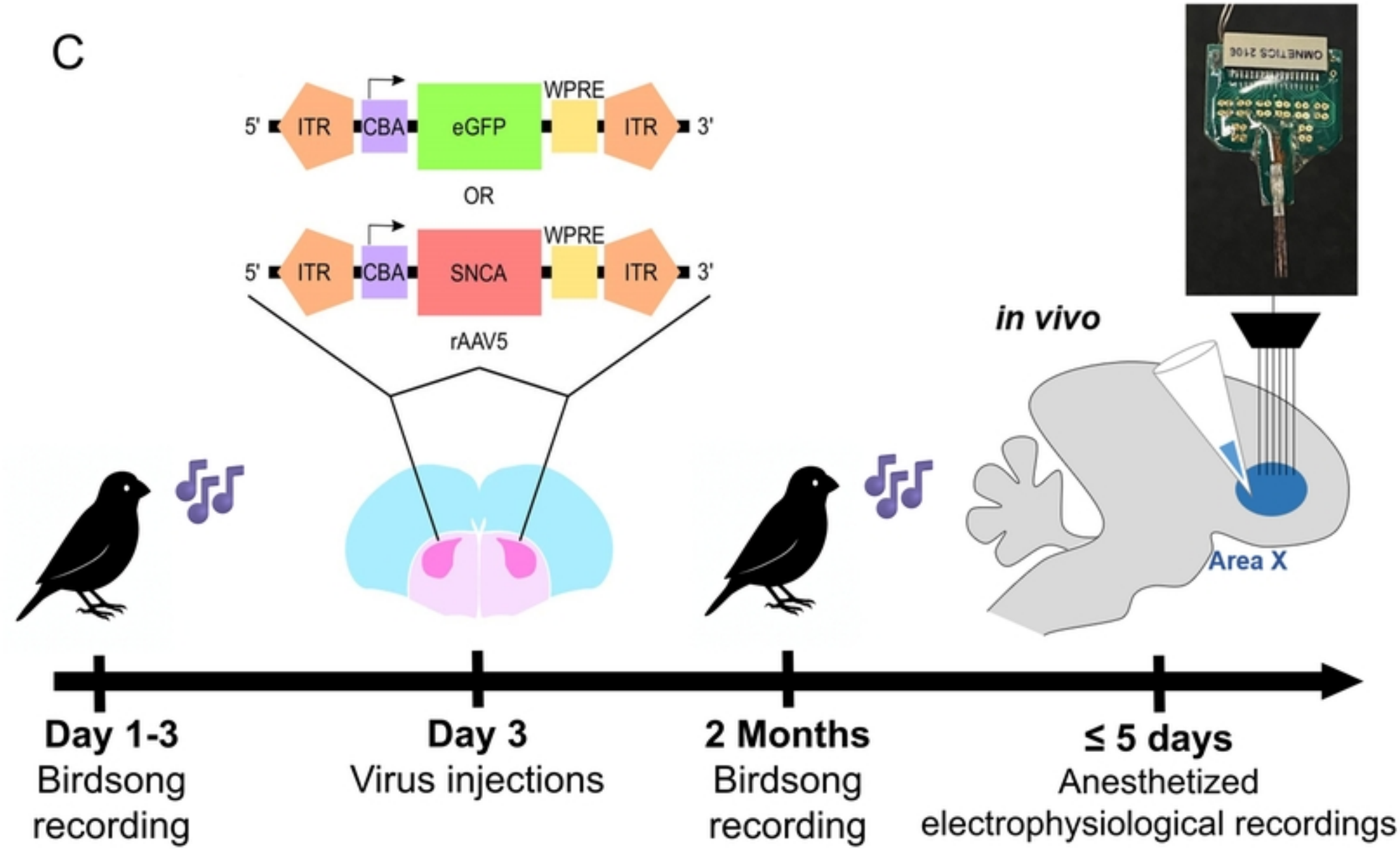
C
5'
ITR
CBA
eGFP
WPRE
ITR
3'
OR
5'
ITR
CBA
SNCA
WPRE
ITR
3'
rAAV5
in vivo
Area X
Day 1-3
Birdsong recording
Day 3
Virus injections
2 Months
Birdsong recording
≤ 5 days
Anesthetized electrophysiological recordings

Figure 1C

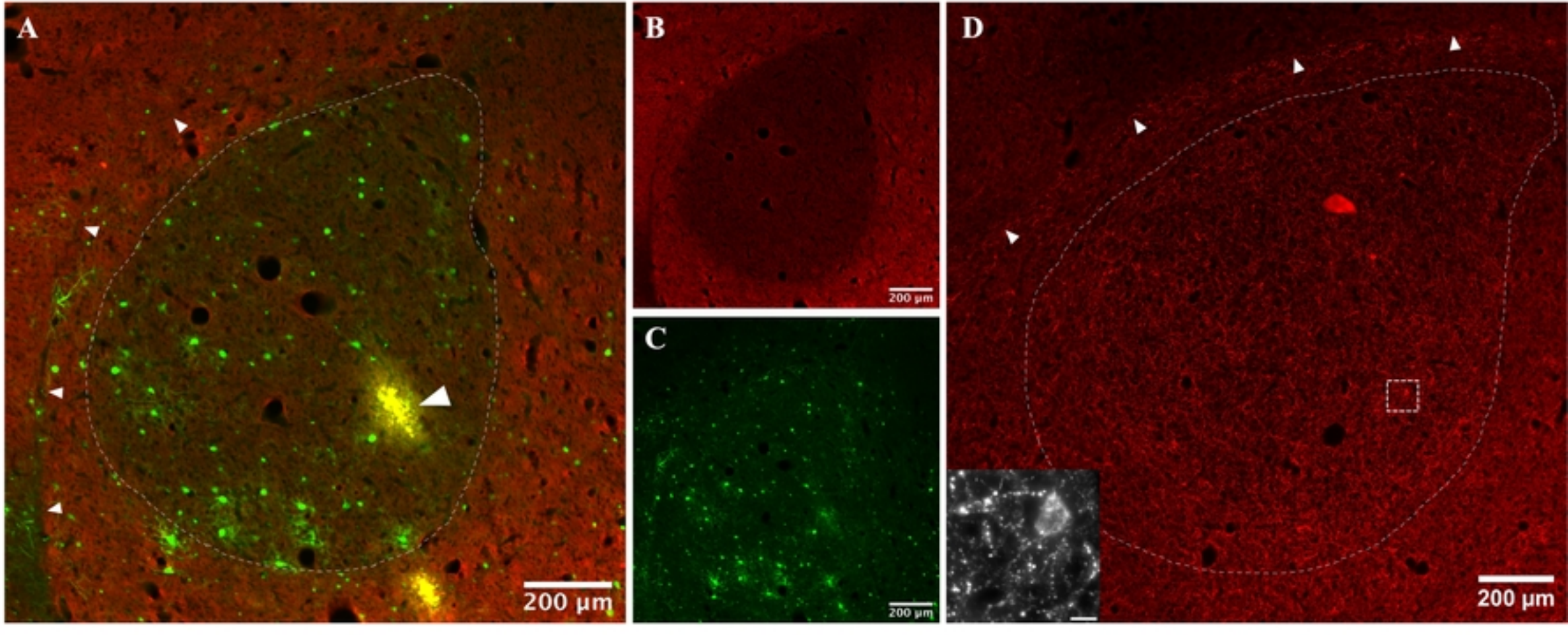

Figure 2

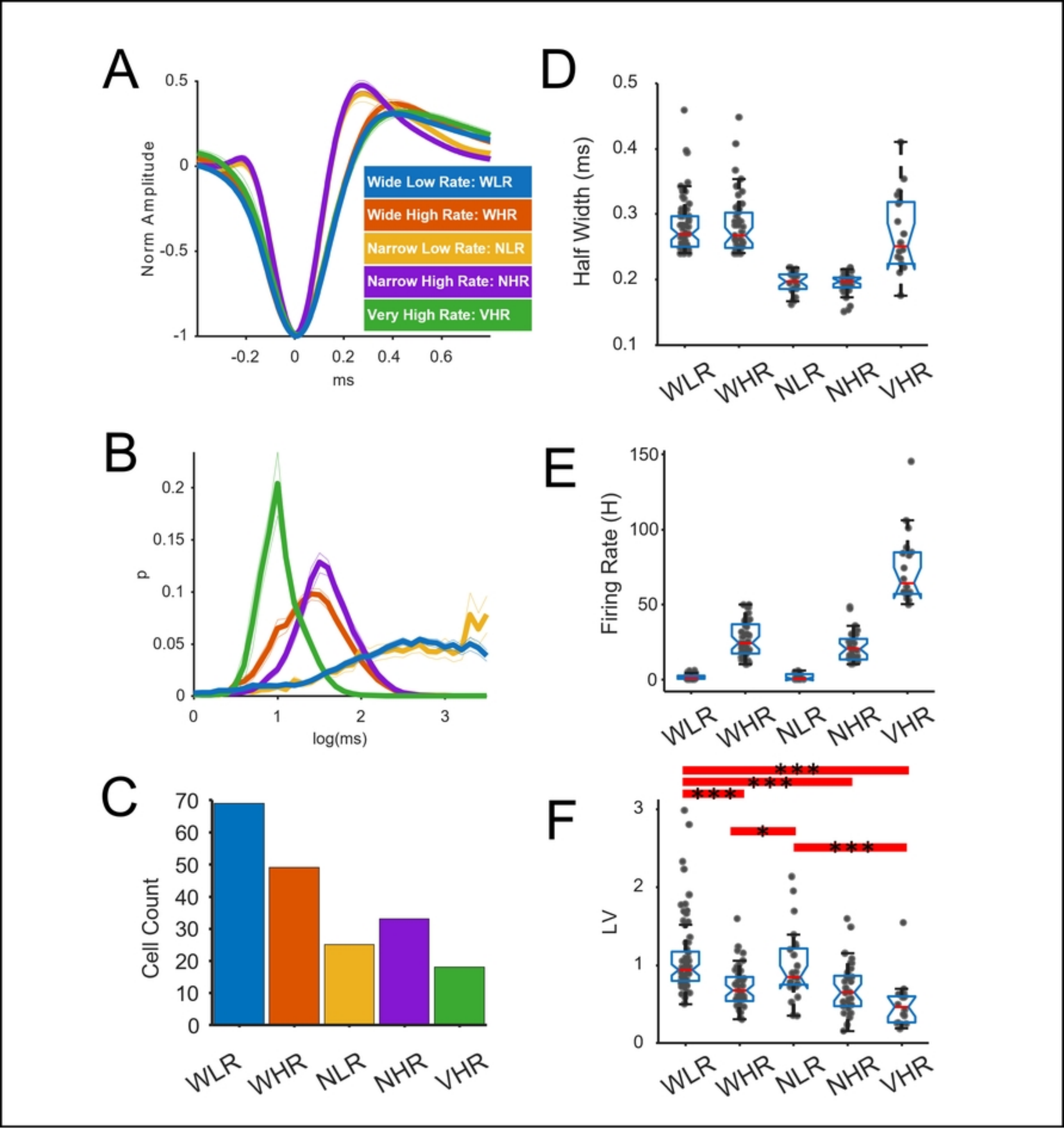
A
Norm Amplitude
ms
Wide Low Rate: WLR
Wide High Rate: WHR
Narrow Low Rate: NLR
Narrow High Rate: NHR
Very High Rate: VHR
B
p
log(ms)
C
Cell Count
WLR
WHR
NLR
NHR
VHR
D
Half Width (ms)
E
Firing Rate (H)
F
LV

Figure 3

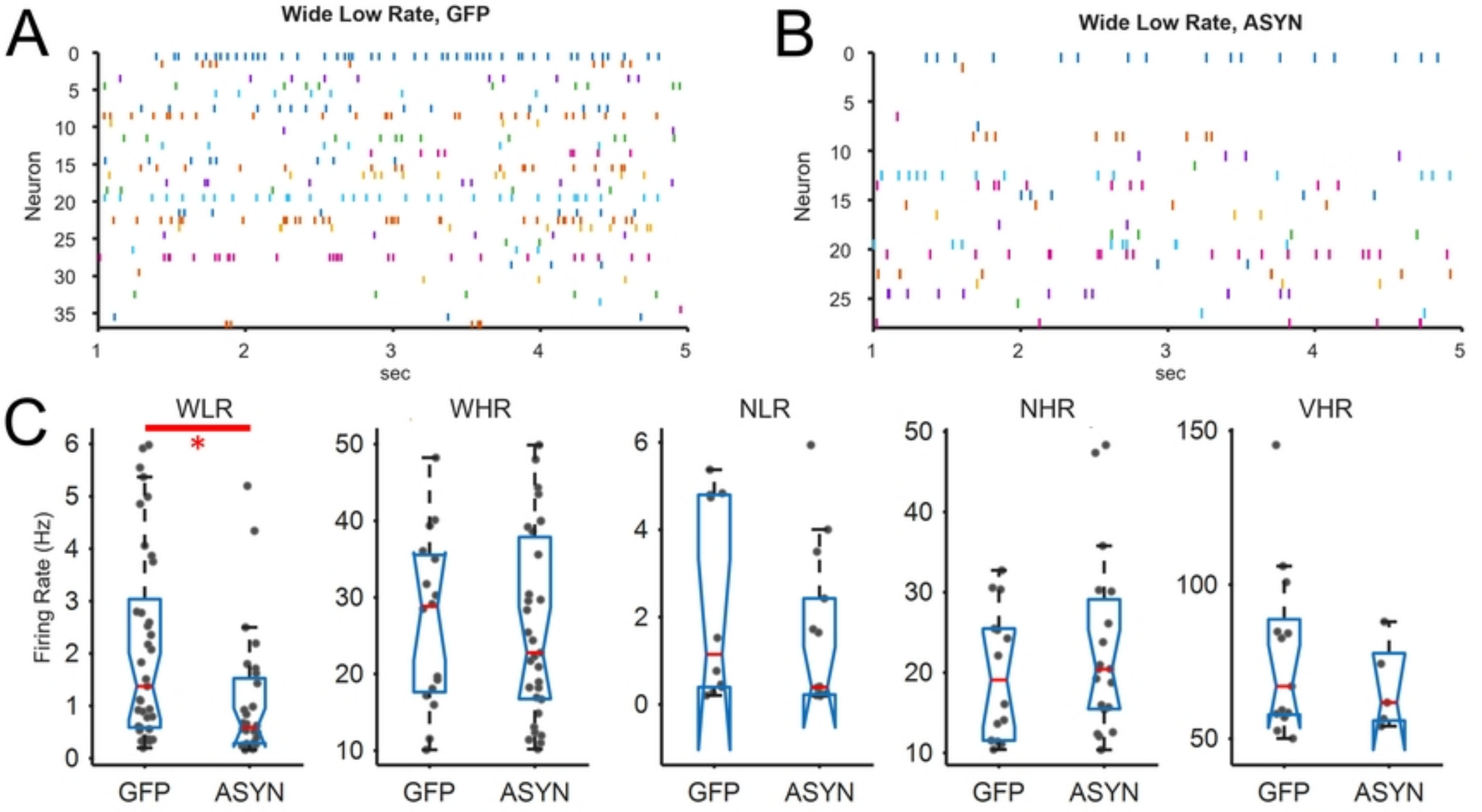
A
Wide Low Rate, GFP
Neuron
sec
B
Wide Low Rate, ASYN
Neuron
sec
C
WLR
WHR
NLR
NHR
VHR
Firing Rate (Hz)
*
GFP
ASYN

Figure 4

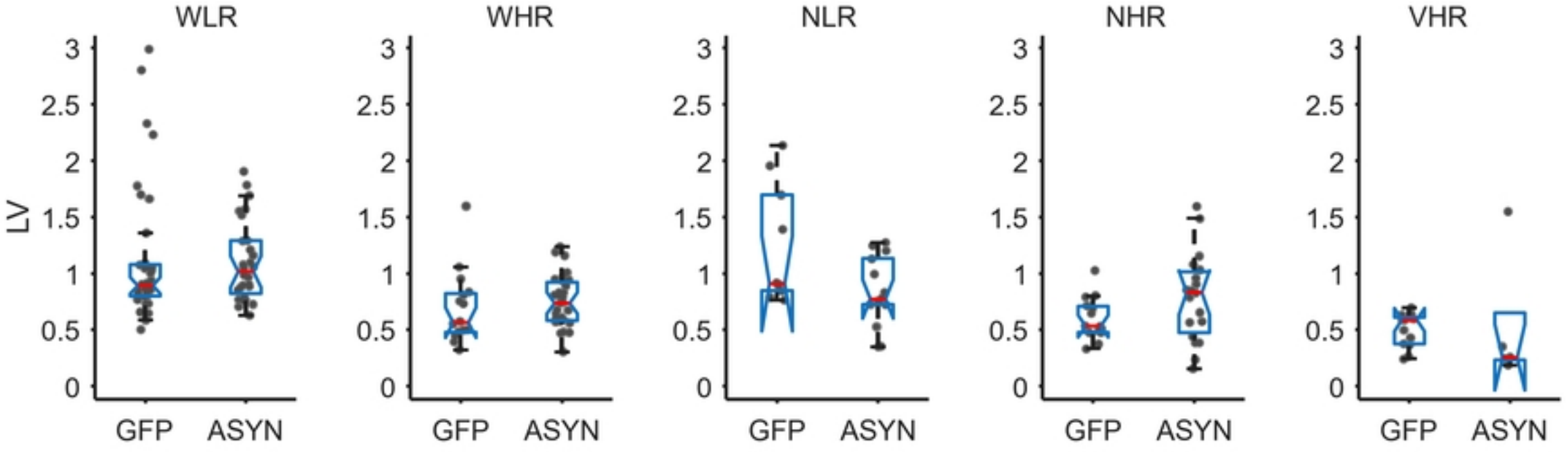

Figure 5

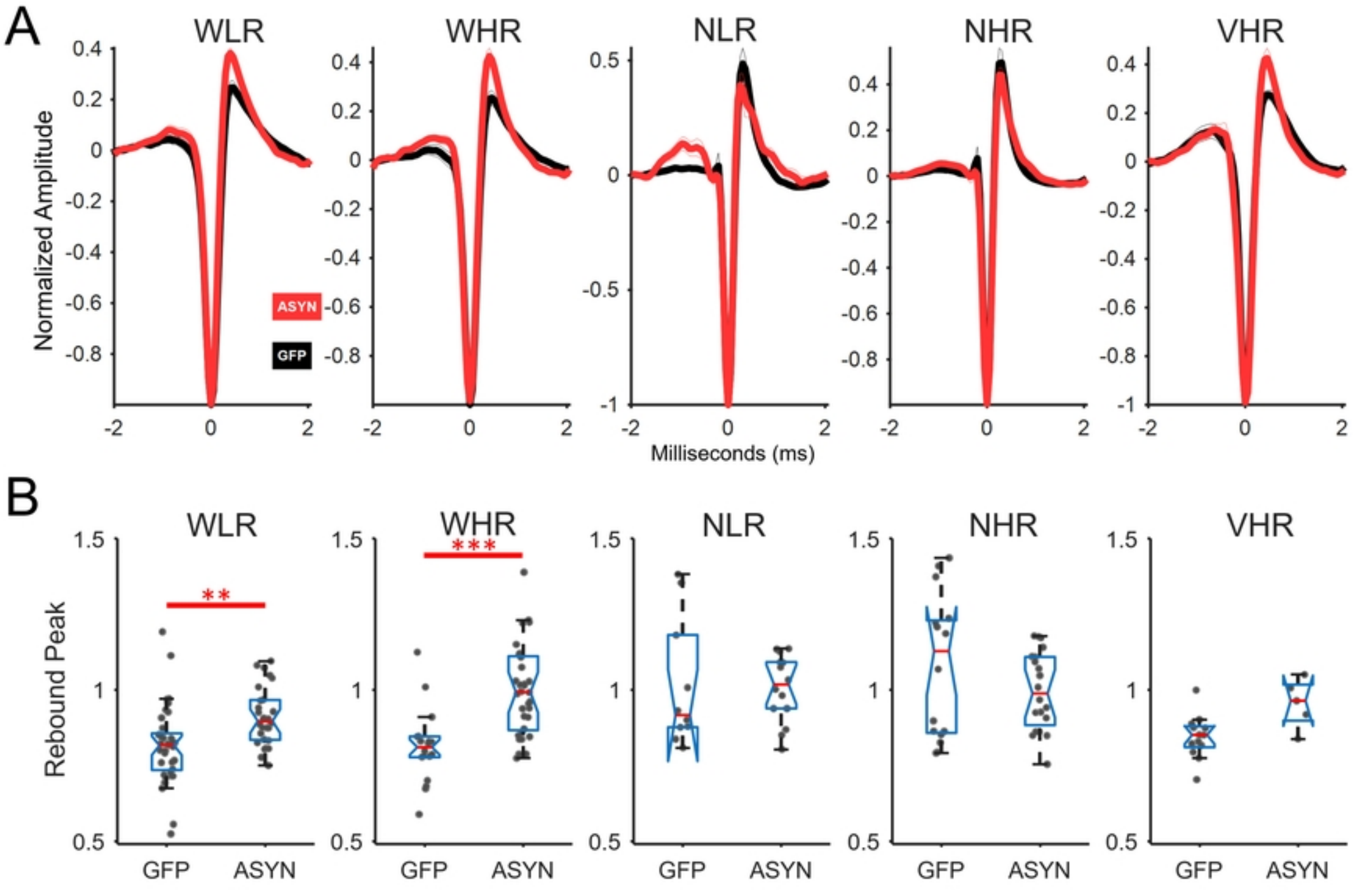
A
WLR
WHR
NLR
NHR
VHR
Normalized Amplitude
ASYN
GFP
Milliseconds (ms)
B
Rebound Peak
**
***
GFP
ASYN

Figure 6

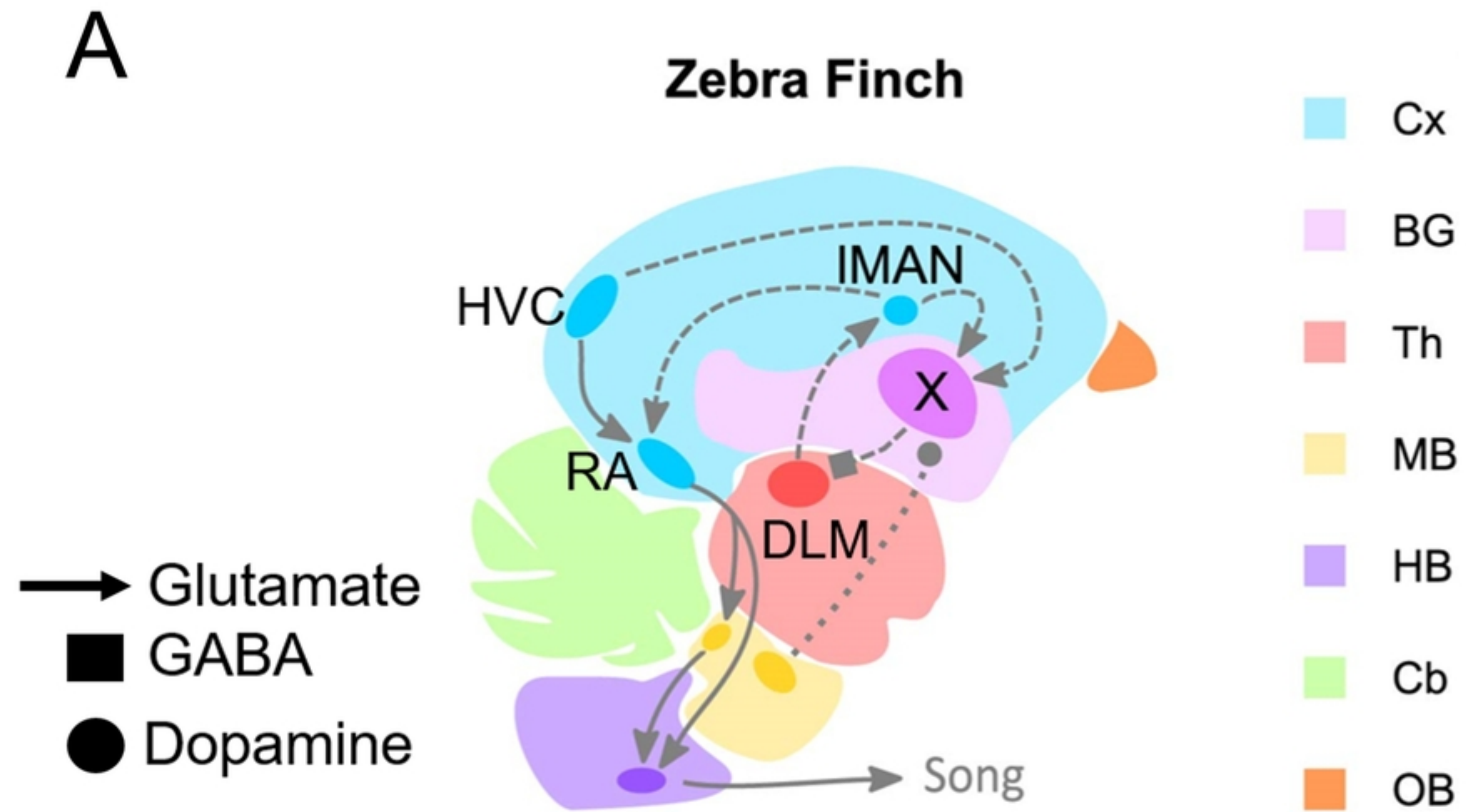
A
Zebra Finch
HVC
IMAN
X
RA
DLM
Song
Glutamate
GABA
Dopamine
Cx
BG
Th
MB
HB
Cb
OB

Figure 1A